J Mater Sci (2014) 49:1476–1483
DOI 10.1007/s10853-013-7917-1

Template-free electrochemical synthesis of tin nanostructures

David T. Mackay · Matthew T. Janish · Uttara Sahaym · Paul G. Kotula · Katherine L. Jungjohann · C. Barry Carter · M. Grant Norton

Received: 8 November 2013 / Accepted: 24 November 2013 / Published online: 6 December 2013

Abstract One-dimensional (1D) nanostructures, often referred to as nanowires, have attracted considerable attention due to their unique mechanical, chemical, and electrical properties. Although numerous novel technological applications are being proposed for these structures, many of the processes used to synthesize these materials involve a vapor phase and require high temperatures and long growth times. Potentially faster methods requiring templates, such as anodized aluminum oxide, involve multiple fabrication steps, which would add significantly to the cost of the final material and may preclude their widespread use. In the present study, it is shown that template-free electrodeposition from an alkaline solution can produce arrays of Sn nanoneedles directly onto Cu foil substrates. This electrodeposition process occurs at 55 °C; it is proposed that the nanoneedles grow via a catalyst-mediated mechanism. In such a process, the growth is controlled at the substrate/nanostructure interface rather than resulting from random plating-induced defects such as dendrites or aging defects such as tin whiskers. There are multiple potential applications for 1D Sn nanostructures—these include anodes in lithium-ion and magnesium-ion batteries and as thermal interface materials. To test this potential, type 2032 lithium-ion battery button cells were fabricated using the electrodeposited Sn. These cells showed initial capacities as high as 850 mAh/g and cycling stability for over 200 cycles.

Introduction

Materials formed as one-dimensional (1D) nanostructures have demonstrated properties that differ greatly from their bulk counterparts, leading to many novel applications [1–5]. As one example, the unique properties of carbon nanotubes could lead to their use in supercapacitors [6], as field emitters [7], and as transistors [8]. Silicon nanowires are another example, with potential applications as field

D. T. Mackay (✉) · U. Sahaym · M. G. Norton
School of Mechanical and Materials Engineering, Washington State University, Pullman, WA 99164, USA
e-mail: dmackay@wsu.edu

U. Sahaym
e-mail: usahaym@wsu.edu

M. G. Norton
e-mail: mg_norton@wsu.edu

M. T. Janish · C. B. Carter
Department of Materials Science and Engineering, University of Connecticut, Storrs, CT 06269, USA
e-mail: matthew.janish@uconn.edu

C. B. Carter
e-mail: cbcarter@engr.uconn.edu

M. T. Janish · C. B. Carter
Institute of Materials Science, University of Connecticut, Storrs, CT 06269, USA

P. G. Kotula · K. L. Jungjohann · C. B. Carter
CINT, Sandia National Laboratories, PO Box 5800, Albuquerque, NM 87185, USA
e-mail: paul.kotula@sandia.gov

K. L. Jungjohann
e-mail: kljungj@sandia.gov

C. B. Carter
Department of Chemical and Biomolecular Engineering, University of Connecticut, Storrs, CT 06269, USA

effect transistors [9] and in catalysis [10]; they have been studied for over 50 years and significant progress has been made in understanding their growth mechanisms [11]. However, methods to fabricate these structures in large quantities and at low temperatures remain elusive. The difficulty of creating a uniform distribution of 1D nanostructures over large surfaces at a low cost prevents large-scale production. Existing processes either do not produce the desired nano-structures uniformly across a large enough area or the fabrication steps involved are too numerous or complex to be economically viable. These challenges are illustrated by the recent work in fabricating Sn nanopillars using electron-beam lithography and electroplating [12].

Many 1D nanostructures, including silicon nanowires (e.g., [11]), are grown via the vapor–liquid–solid (VLS) mechanism that was first described by Wagner and Ellis [13]. The key aspect of the VLS mechanism is a liquid (L) catalyst cap through which the vapor (V) passes before it forms as a solid (S) on a suitable substrate surface. Since the original work on VLS in the 1960s, this mechanism has been identified in the growth of many 1D nanostructures, e.g., [14–16], which illustrate the versatility of the process. However, the requirements of a liquid catalyst and reactants in the vapor phase generally necessitate that any process involving the VLS growth mechanism be conducted at high temperature. Similar processes have been identified for a solid cap but it is not known how widely this occurs (e.g., [17]). For Si nanowires using an Au catalyst the growth temperature is typically $\sim$500 °C (e.g., [18]). For carbon nanotubes using a Ni catalyst the growth temperature is >800 °C (e.g., [19]). Growth of 1D nanostructures by VLS frequently demands an inert atmosphere and universally suffers from low growth rates. Such limitations make it an expensive and slow process, neither of which are traits conducive to commercial-scale applications.

One-dimensional nanostructures can also be fabricated by electroplating with the assistance of a template. Anodic aluminum oxide (AAO) is a popular template and has been used for fabricating Sn nanowires (e.g., [20, 21]). In one example of this method, aluminum foil is used as the starting step. The aluminum is soaked in an $HgCl_2$ solution to create nanoscale holes throughout the bulk material. The underlying metal is exposed by etching in a phosphoric acid solution at 32 °C for 60 min. Tin is electrodeposited into the holes creating nanowires at a constant current density of 0.75 mA/cm^2. The template is finally removed by wet etching by 0.5 M NaOH leaving only Sn nanowires [20]. Drawbacks of this approach are the extra steps involved in preparing and then removing the template, as well as the time and resources required to do so.

This paper describes the development of a template-free electroplating process that can be used to form arrays of 1D Sn nanostructures ("nanoneedles") directly on Cu substrates under very mild synthesis conditions at 55 °C. Electroplating is a well-understood process and has a small number of fabrication steps [22]. Therefore, it is an advantageous method for producing large areas of Sn nanoneedles directly on suitable substrates. Tin nanostructures have potential uses as advanced thermal interface materials [23]; as anodes in lithium-ion [24], magnesium-ion [25], and sodium-ion batteries [26]; and as a nano-soldering material [27].

Experimental

Tin nanoneedles were synthesized by electrodeposition from an alkaline Sn solution directly onto 1 cm × 0.7 cm × 0.75 mm copper substrates (99.99 % pure, Alfa Aesar, Ward Hill, MA, USA) as described in detail elsewhere [28]. The solution was prepared by dissolving approximately 3 g of sodium hydroxide and 28 g of sodium stannate trihydrate in deionized water to make 200 ml of solution. Copper substrates were prepared by cutting and polishing 1 cm × 1 cm × 0.75 mm coupons using standard metallographic procedures. After polishing, the substrates were cleaned using a 9.4 M NaOH solution and immersed for 15 s in sulfuric acid to remove the surface oxide layer. Prior to electrodeposition, the Cu substrate and stainless steel counter-electrode coupons were placed 2.5 cm apart and immersed in the electroplating solution for 30 min. A 0.7 cm^2 area of each electrode was pre-soaked in this way. Tin was electrodeposited onto the soaked region of the Cu electrode at a voltage of 2.4 V and current density of 35 mA/cm^2 at 55 °C for 11 min. A magnetic stir-bar (2.5 cm long) was used to agitate the solution at 320 rpm. These parameters were chosen based on our previous study to yield the most uniform density of nanoneedles on the copper substrate [28].

Using the same process, Sn nanoneedles were formed on 10 mm × 10 mm × 10 μm thick TLB-DS and TLB-PLSP Cu foils (Oak Mitsui, Hoosick Falls, New York). Both TLB-PLSP and TLB-DS are commercial electrodeposited Cu foils specifically designed for lithium-ion battery applications. The TLB-DS foil is characterized by a Cu nodule treatment on the surface that was developed to improve coating reliability and to enhance adhesion. The TLB-PLSP does not have this treatment and consequently has a smoother surface (115 μ in. compared to 125 μ in.). Both of these foil samples were used as-received from the manufacturer, without cleaning with sodium hydroxide solution and sulfuric acid, in order to avoid altering the properties of this texturing.

The plated Cu substrates were assembled into type 2032 button cells in a dry, argon-filled glove box using Li as the counter electrode and a semi-permeable polyethylene separator. The electrolyte was a 1 M lithium hexafluorophosphate solution, with a 1:1:1 ethylene carbonate (EC), dimethyl carbonate (DMC), and diethyl carbonate (DEC) organic solvent. The cells were cycled between 0 and 3 V under charging and discharging currents of 0.05 mA, or 0.08 mA/cm^2 using a BST8-WA battery analyzer.

Microstructural characterization of as-deposited and subsequently tested nanostructures was conducted using an FEI Quanta 200F field-emission scanning electron microscope (SEM) operated at 20 kV, an FEI Tecnai F30 transmission electron microscope (TEM) operated at 300 kV, an FEI Titan G2 80-200 equipped with Chemi-STEM Technology operated at 200 kV, and a Zeiss Supra 55VP FESEM equipped with a Bruker silicon-drift detector (SDD) operated at 10 kV.

Results and discussion

Figure 1a is a SEM image illustrating the typical coverage of Sn nanoneedles on the copper substrate. The Sn nanoneedles vary in size and orientation creating an open network across the entire substrate surface. The total mass of Sn electrodeposited under the experimental conditions described above is approximately 1 mg (or 1.43 mg/cm^2). Figure 1b shows a higher-magnification SEM image of a cluster of Sn nanoneedles. Typical nanoneedle dimensions are: length 1–5 μm, tip-width 20–100 nm, and base-width 50–300 nm. The distinguishing characteristic of a nanoneedle, as opposed to a nanowire, is the tapering of the structure along its length. Two important characteristics of these nanoneedles are highlighted in Fig. 1b: first, many of them appear to end in a facetted cap; second, the growth process leads to multiple branch points where two or more new nanoneedles grow from an existing nanoneedle stem. The cap is also visible in the bright-field TEM image in Fig. 2.

The tapered structure and the presence of the facetted nanoparticle cap distinguish these electrodeposited nanoneedles from commonly found electroplating defect structures and the ubiquitous Sn whiskers. Tin whiskers are filamentary monocrystalline structures that grow from deposited films (e.g., [29]). Whiskers always form after plating and have an incubation period that can vary from days to years. Dendrites are defects that form during the plating process when the Sn crystallizes in a branching or tree-like structure [29]. Unlike Sn whiskers, dendrites are always polycrystalline and typically show a pointed tip [29]. The most common cause of Sn dendrites during plating is insufficient surfactant concentration [29]. Tin

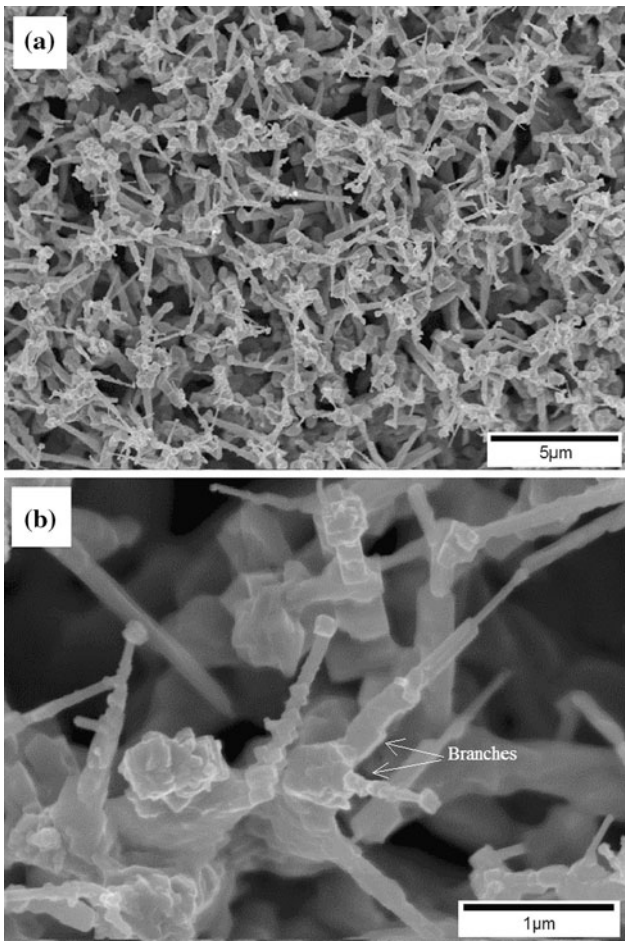

Fig. 1 **a** SEM image showing tin nanoneedles formed by electroplating onto copper substrates. **b** Higher-magnification image of the same sample showing branch points formed during nanoneedle growth

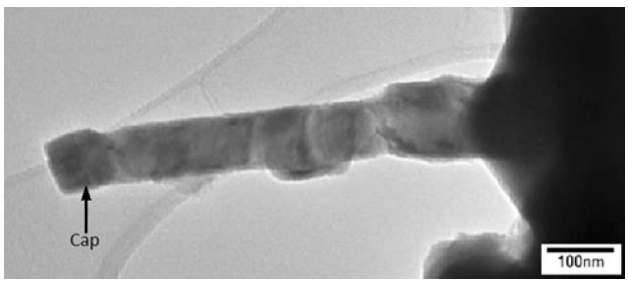

Fig. 2 Bright field TEM image of an individual tin nanoneedle

needles have been observed as a plating defect [30]. Typically they are much larger (widths tapering from ~5–2 μm and lengths >50 μm) than the nanoneedles described in the present study and appear to form as random defects on an otherwise uniform Sn film. The presence of the facetted cap at the tip of each Sn nanoneedle suggests that the growth process may be controlled by this structure in a manner analogous to the role of the liquid

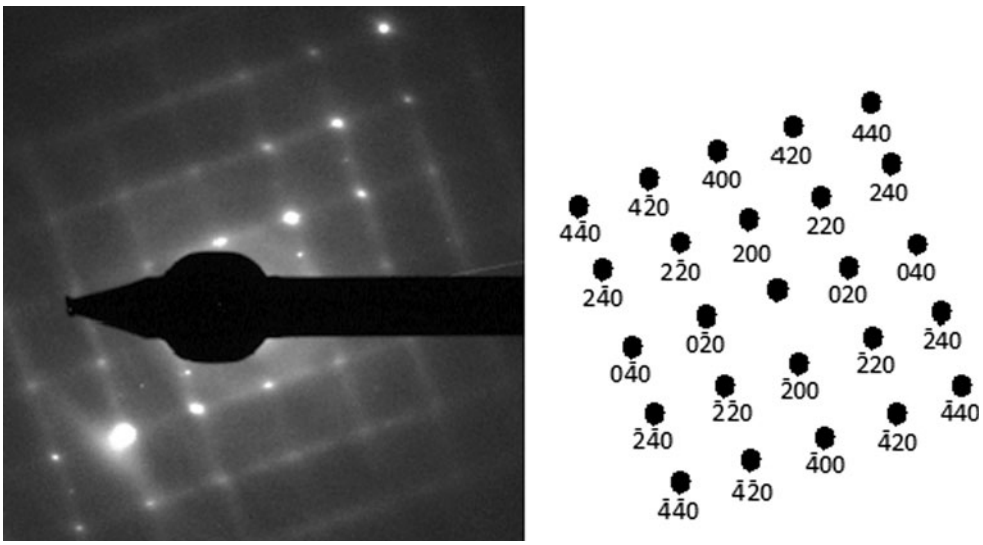

Fig. 3 Electron diffraction pattern from an individual tin nanoneedle. The schematic shows the indexing to β-Sn. The unlabeled reflections are also due to β-Sn and possibly arise from emergent branch points on the nanoneedle surface

catalyst in the VLS process. In this event, the growth of the nanoneedles would involve both a nucleation stage and a growth stage and is possibly catalyst-assisted. The branching of nanoneedles from a central stem, illustrated in Fig. 1b, also suggests that new nucleation sites appear during the growth of nanoneedles that have already nucleated.

Energy-dispersive X-ray spectroscopy (XEDS) analysis (results not shown) indicates that the nanoneedles are composed of pure tin, possibly with a thin native oxide on the surface. Selected-area diffraction (SAD) patterns from individual nanoneedles observed in the transmission electron microscope (TEM) confirm that they are single crystal β-Sn (Fig. 3).

The proposed growth mechanism of the Sn nanoneedles is based on SEM observations of the Cu substrate surface after the pre-deposition soak and after electroplating for short durations. Figure 4a is an SEM image of the surface of a Cu substrate after it had been soaked in the electrolyte for 30 min (the incubation period prior to electrodeposition). During the experiment, the color of the substrate changed visibly from the characteristic yellow of copper to red, which is associated with cuprous oxide (Cu_2O). It is clear from the figure that this oxide layer takes the form of cubes that provide texture to the surface and vary in size from several tens of nanometers to 1 μm. Tin structures formed on the surface as soon as deposition began, as illustrated in the micrograph shown in Fig. 4b. It is not clear if there are preferential sites on the cube surface (e.g., faces, edges, corners) for nucleation; further studies are in progress to determine, more specifically, the details of the nucleation process. What is clear is that subsequent deposition leads to the formation of the capped nanoneedles and that the size of the caps is similar to the Sn islands formed on the cuprous oxide cubes. The process is illustrated

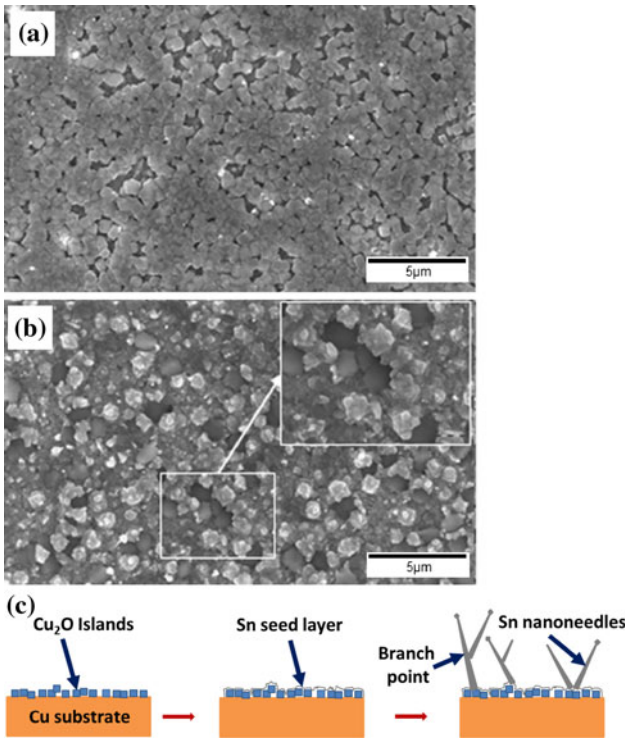

Fig. 4 Stages in the growth of tin nanoneedles. **a** SEM image showing the surface of a copper substrate after being soaked (in the electrolyte) for 30 min. **b** SEM image of the initial tin seed layer formed during electrodeposition. **c** Schematic of the proposed growth mechanism of the nanoneedles

schematically in Fig. 4c; it is proposed that the Sn nanoparticles act as the catalyst for the growth of the nanoneedles. Growth of the nanoneedles continues as long as there is a supply of Sn ions from the solution to the solid catalyst.

Based on the above observations, the following mechanism is proposed for the formation of Sn nanoneedles that

can be described as "liquid–solid–solid" or LSS. Tin ions are the basic building blocks and are provided from the liquid phase; both the catalyst and the final nanostructure are in the solid phase. This mechanism can be compared, in some respects, to the self-catalyzed growth of SnO_2 observed by Wang et al. [31]. The SnO_2 nanowires grow by the VLS mechanism without any foreign metallic catalyst. The proposed LSS mechanism is not to be confused with the solid–liquid–solid (SLS) mechanism that has been used to explain the growth of, e.g., single wall nanotubes (SWNT) [32]. In the SLS mechanism the catalyst is liquid and the carbon source for SWNT growth is amorphous carbon condensed on the catalyst drop.

The proposed LSS mechanism is complicated by the electric field applied during the electrodeposition process. The Sn nanoparticles experience higher current densities compared to the average surface or neighboring recesses, which provides favorable sites for the rapid supply of Sn ions by diffusion [33]. This results in the formation of the observed nanoneedles rather than a smooth Sn film.

Template-free electrodeposition techniques have been demonstrated for synthesis of several other 1D nanostructures including ZnO [34], Te [35], and copper telluride [36]. Zinc oxide columns with diameters between 100 and 200 nm and several microns in length have been fabricated by electrodeposition from a zinc chloride solution onto tin oxide substrates. These columns have potential use in the semiconductor industry as a substrate for Si deposition [34]. Tellurium nanowires have been electroplated at low synthesis temperatures (85 °C) in an alkaline tellurium solution onto glass coated with indium tin oxide (ITO). Understanding the fabrication of these tellurium nanowires can give broader insights into template-free electroplating techniques [35]. Copper telluride nanoribbons have also been electroplated from an alkaline solution onto indium tin oxide coated glass: these nanoribbons may have applications as gas sensors [36].

The LSS mechanism proposed here may be a major player in template-free electrodeposition, and if so will have broader applications in creating large area, low-cost arrays of nanostructures of other metals. For example, Mo nanowire arrays have potential application as cold cathode electron emitters for field-emission arrays [37]. Zhou et al. have produced large area coatings of molybdenum nanowires on stainless steel substrates that look morphologically similar to the Sn nanostructures produced here by electrodeposition. However, the chemical vapor deposition (CVD) process used by Zhou et al. [38] requires temperatures in excess of 1600 K. Using electrodeposition at temperatures close to room temperature would significantly decrease the cost of producing these nanostructures in volume.

Arrays of Sn nanostructures have attracted interest recently as an anode material for lithium-ion batteries (e.g., [39, 40]). Tin has a theoretical specific capacity of 994 mAh/g, which is more than 2.5 times greater than that of carbon. Unfortunately, attempts to use Sn as an anode have met significant obstacles. Because Sn undergoes a volume expansion of 300 % during the lithiation and delithiation process, Sn anodes have previously suffered from a poor cycle life compared to carbon anodes [40]. After 10–20 cycles, the stresses caused by the expansions and contractions begin to degrade the battery, cracking and separating the anode material from the current collector. Recent work has focused on two methods of overcoming this limitation: by dispersing the Sn in a matrix phase that can accommodate the changes in volume during cycling [41–44], and by forming the Sn (or its oxides or alloys) as one-, two-, or three-dimensional nanostructures [45–48]. In the latter case, the stresses are reduced by providing the electrode with free space to expand and contract during cycling. This approach has been successfully demonstrated with Si, for which the volumetric change is even greater than that of Sn (e.g., [18]). Some materials use a combination of both methods for overcoming the volume change [49]. The Sn nanoneedles described in this study have demonstrated similar performance to all of these advanced materials, with the added advantages of ease of fabrication and industrial scalability.

Figure 5a shows the capacity-cycling curve for a typical Sn nanoneedle anode. The initial discharge capacity is typically in the range 400–500 mAh/g, though values as high as 850 mAh/g have been achieved. The initial discharge capacity decreases slightly during the first 20 cycles, and after reaching a minimum begins to increase and stabilizes around 600 mAh/g after 40 additional cycles. This behavior appears to be an unusual characteristic for Sn anodes, but it has been noted for cells using composite silicon-based anodes [50]. The implication of such behavior is that during the first 60 cycles the anode undergoes some structural, morphological, or chemical change. Future testing will be needed to determine the exact processes that occur during cycling, but the initial results are very promising. Figure 5b is an SEM image showing an example of the Sn nanoneedles after cycling within a battery. The nanoneedles appear to have retained their structural integrity after 100 charge/discharge cycles. In contrast, many other Sn-based anodes experience dramatic cracking under similar cycling conditions (see, e.g., [51]). Based on results with present test cells, the Sn anodes remain intact for up to 200 cycles and longer-term tests are currently underway. These results support the broader implication of the work by Chan et al. [18] that 1D nanostructures can accommodate the volume expansion and contraction during lithiation and delithiation.

Figure 6 is an SEM image of the Sn nanoneedles formed on the TLB-PLSP Cu foil sample. Although the nanoneedles

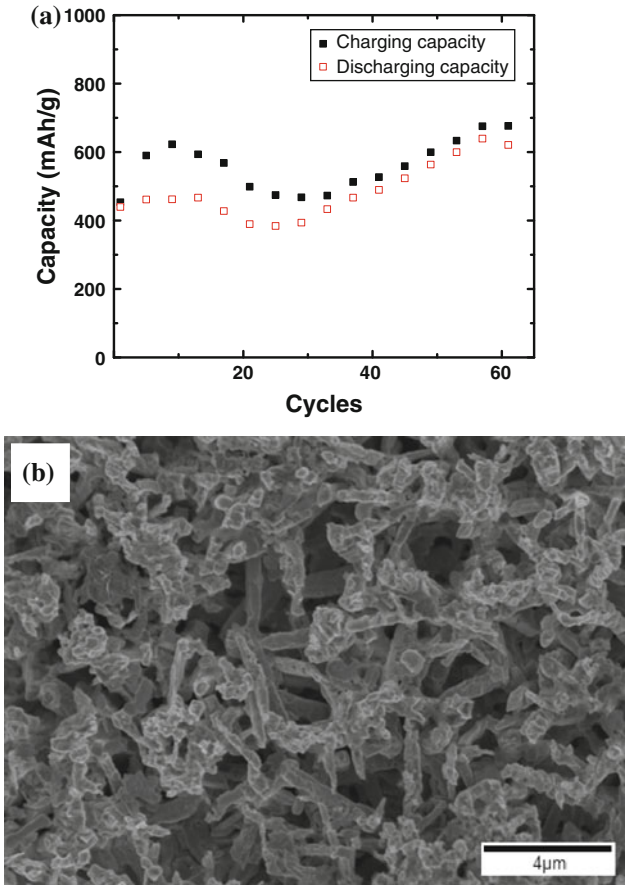

Fig. 5 **a** Capacity-cycling plot of a button cell using a tin nanoneedle anode. **b** SEM image of a tin nanoneedle anode after 100 lithiation/delithiation cycles

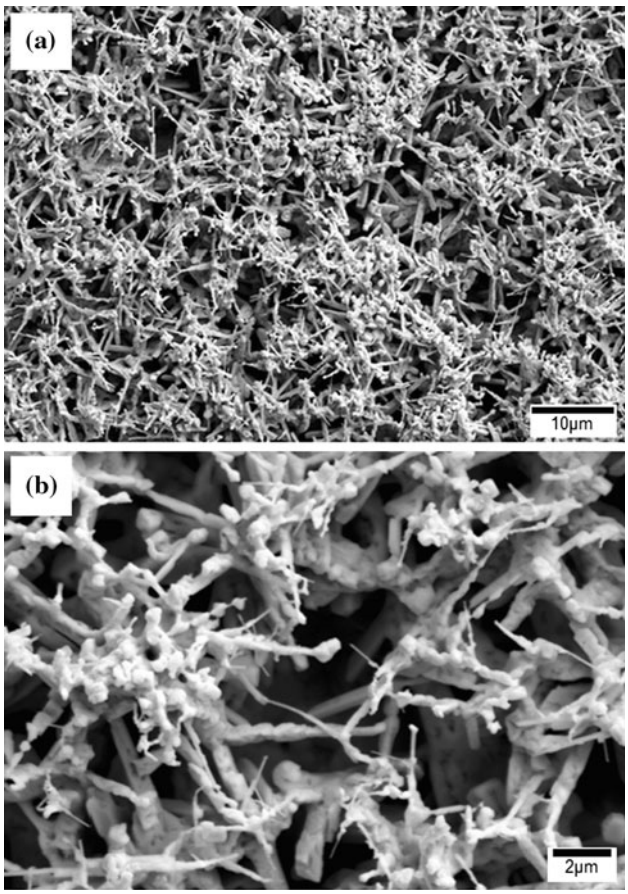

Fig. 6 **a** SEM image of tin nanoneedles formed onto copper tape. **b** The same sample at higher-magnification showing that the nanoneedle morphology is very similar to that formed on the thicker copper substrates

appeared similar to those formed on the thicker copper substrates, they were generally narrower with a denser surface coverage. These results show that the electrodeposition process works equally well for Cu substrates and thinner Cu foils. The latter case represents the typical form of the current carrier used in commercial lithium-ion batteries. In addition, the method can be used to form Sn nanoneedles by electrodeposition onto Cu foils with dimensions 6 cm × 6 cm, the size needed for fabricating prismatic cells (i.e., SCP-42LBPS) and foils as large as 66 cm × 6 cm. The latter allow fabrication of 18650 cells—the typical geometry used in many laptop computer batteries. These results demonstrate that the electrodeposition process for forming the Sn nanoneedles is industry-scalable.

Conclusions

A new method for the synthesis of a 1D Sn nanostructured material by electrodeposition without using a template has been described. The monocrystalline β-phase Sn nanoneedles can be formed directly on Cu substrates, which are the typical current carrier in lithium-ion batteries. The proposed growth mechanism for the Sn nanoneedles is a liquid–solid–solid (LSS) process, a catalyst-mediated process that involves Sn nanoparticles nucleating on the substrate surface in the early stages of electrodeposition. In this paper, we demonstrated one potential application for the Sn nanoneedles as anodes for lithium-ion batteries. Initial capacities of around 850 mAh/g have been achieved in button-sized cells. Importantly, the electrodeposition process is scalable and in this study we have shown that Sn nanoneedle arrays can be formed on Cu foils as large as 66 cm × 6 cm.

Acknowledgements This work was supported, in part, by the Washington Research Foundation and the Office of Research at Washington State University. A part of this work was performed at the Center for Integrated Nanotechnologies, a DOE-BES supported national user facility. Sandia is a multiprogram laboratory operated by Sandia Corporation, a Lockheed Martin Company, for the United States Department of Energy's (DOE) National Nuclear Security Administration (NNSA) under contract DE-AC0494AL85000. Matthew Janish is partly supported by a GAANN Fellowship from the US Department of Education. Discussions with Joseph R. Michael, Bonnie McKenzie, and Summer R. Ferreira are gratefully acknowledged.

References

1. Spencer M (2012) Gas sensing applications of 1D-nanostructured zinc oxide: Insights from density functional theory calculations. Prog Mater Sci 57:437–486
2. Zhai T, Fang X, Li L, Bando Y, Golberg D (2010) One-dimensional CdS nanostructures: synthesis, properties, and applications. Nanoscale 2:168–187
3. Tian J, Xu Z, Shen C, Liu F, Xu N, Gao H-J (2010) One-dimensional boron nanostructures: prediction, synthesis, characterizations, and applications. Nanoscale 2:1375–1389
4. Guo MY, Fung MK, Fang F, Chen XY, Ng AMC, Djurisic AB, Chan W (2011) ZnO and TiO_2 1D nanostructures for photocatalytic applications. J Alloys Compd 509:1328–1332
5. Koenigsmann C, Wong S (2011) One-dimensional noble metal electrocatalysts: a promising structural paradigm for direct methanol fuel cells. Energy Environ Sci 4:1045–1528
6. Kim B, Chung H, Kim W (2012) High-performance supercapacitors based on vertically aligned carbon nanotubes and nonaqueous electrolytes. Nanotechnology 23:155401
7. Doytcheva M, Kaiser M, De Jonge N (2006) In situ transmission electron microscopy investigation of the structural changes in carbon nanotubes during electron emission at high currents. Nanotechnology 17:3226–3233
8. Cao Q, Rogers J (2009) Ultrathin films of single-walled carbon nanotubes for electronics and sensors: a review of fundamental and applied aspects. Adv Mater 21:29–53
9. Duan X, Niu C, Sahi V, Chen J, Parce J, Empedocles S, Goldman J (2003) High-performance thin-film transistors using semiconductor nanowires and nanoribbons. Nature 425:274–278
10. Tsang C, Liu Y, Kang Z, Ma D, Wong N, Lee S (2009) Metal (Cu, Au)-modified silicon nanowires for high-selectivity solvent-free hydrocarbon oxidation in air. Chem Comm 39:5829–5831
11. Schmidt V, Wittemann J, Senz S, Gosele U (2009) Silicon nanowires: a review on aspects of their growth and their electrical properties. Adv Mater 21:2681–2702
12. Burek M, Budiman A, Jahed Z, Tamura N, Kunz M, Jin S, Han S, Lee G, Zamecnik C, Tsui T (2011) Fabrication, microstructure, and mechanical properties of tin nanostructures. Mater Sci Eng A 528:5822–5832
13. Wagner R, Ellis W (1964) Vapor–liquid–solid mechanism of single crystal growth. Appl Phys Lett 4:89–90
14. McIlroy D, Zhang D, Kranov Y, Norton M (2001) Nanosprings. Appl Phys Lett 79:1540–1542
15. Panda D, Tseng T (2013) One-dimensional ZnO nanostructures: fabrication, optoelectronic properties, and device applications. J Mater Sci 48:6849–6877. doi:10.1007/s10853-013-7541-0
16. Thabethe B, Malgas G, Motaung D, Malwela T, Arendse C (2013) Self-catalytic growth of tin oxide nanowires by chemical vapor deposition process. Nanomater. doi:10.1155/2013/712361
17. Kodambaka S, Tersoff J, Reuter M, Ross F (2007) Germanium nanowire growth below the eutectic temperature. Science 316:729–732
18. Chan C, Peng H, Liu G, McIlwrath K, Zhang X, Huggins R, Cui Y (2008) High-performance lithium battery anodes using silicon nanowires. Nat Nanotechnol 3:31–35
19. Kukovitsky E, L'vov S, Sainov N (2000) VLS-growth of carbon nanotubes from the vapor. Chem Phys Lett 317:65–70
20. Chen C, Bisrat Y, Luo Z, Schaak R, Chao C, Lagoudas D (2006) Fabrication of single-crystal tin nanowires by hydraulic pressure injection. J Nanotechnol 17:367–374
21. Djenizian T, Hanzu I, Eyraud M, Santinacci L (2008) Electrochemical fabrication of tin nanowires: a short review. C R Chim 995–1003:995–1003
22. Schlesinger M, Paunovic M (2010) Modern electroplating. Wiley, Hoboken
23. Minzarik D, Jellesen M, Moller P, Wahlberg P, Ambat R (2009) Electrochemical migration on electronic chip resistors in chloride environments. IEEE Trans Device Mater Reliab 9:392–402
24. Feng B, Faruque F, Bao P, Chien A, Kumar S (2013) Double-sided tin nanowire arrays for advanced thermal interface materials. Appl Phys Lett. doi:10.1063/1.4791575
25. Singh N, Arthur T, Ling C, Matsui M, Mizuno F (2013) A high energy-density tin anode for rechargeable magnesium-ion batteries. Chem Commun 49:149–151
26. Zhu H, Jia Z, Chen Y, Weadock N, Wan J, Vaaland O, Han X, Li T, Hu L (2013) Tin anode for sodium-ion batteries using natural wood fiber as a mechanical buffer and electrolyte reservoir. Nano Lett 13:3093–3100
27. Cui Q, Rajathurai K, Jia W, Li X, Gao F, Lei Y, Gu Z (2010) Synthesis of single crystalline tin nanorods and their application as nanosoldering materials. J Phys Chem C 114:21938–21942
28. Sahaym U, Miller S, Norton M (2010) Effect of plating temperature on Sn surface morphology. Mater Lett 64:1547–1550
29. LeBret J, Norton M (2003) Electron microscopy study of tin whisker growth. J Mater Res 18:585–593
30. Zhang Y (2010) Physical description. In: Schlesinger M, Paunovic M (eds) Modern electroplating. Wiley, Hoboken, pp 169–172
31. Wang B, Yang Y, Wang C, Yang G (2005) Nanostructures and self-catalyzed growth of SnO_2. J Appl Phys 98:073520-1–073520-5
32. Gorbunov A, Jost O, Pompe W, Graff A (2002) Solid–liquid–solid growth mechanism of single-wall carbon nanotubes. Carbon 40:113–118
33. Bockris JOM, Razumney G (1967) Fundamental aspects of electrocrystallization. Plenum Press, New York
34. Konenkamp R, Boedecker K, Lux-Steiner M, Poschenrieder M, Zenia F, Levy-Clement C, Wagner S (2000) Thin film semiconductor deposition on free-standing ZnO columns. Appl Phys Lett 77:2575–2577
35. She G, Shi W, Zhang X, Wong T, Cai Y, Wang N (2009) Template-free electrodeposition of one-dimensional nanostructures of tellurium. Cryst Growth Des 9:663–666
36. She G, Zhang X, Shi W, Cai Y, Wang N, Liu P, Chen D (2008) Template-free electrochemical synthesis of single-crystal CuTe nanoribbons. Cryst Growth Des 8:1789–1791
37. Spindt C, Brodiel I, Humphrey L, Westerberg E (1976) Physical properties of thin-film field emission cathodes with molybdenum cones. J Appl Phys 47:5248–5263
38. Zhou J, Deng S, Gong L, Ding Y, Chen J, Huang J, Chen J, Xu N, Wang Z (2006) Growth of large-area aligned molybdenum nanowires by high temperature chemical vapor deposition: synthesis, growth mechanism, and device application. J Phys Chem B 110:10296–10302
39. Kamili A, Fray D (2011) Tin-based materials as advanced anode materials for lithium ion batteries. Rev Adv Mater Sci 27:14–24
40. Park C, Kim J, Kim H, Sohn H (2010) Li-alloy based anode materials for Li secondary batteries. Chem Soc Rev 39:3115–3141
41. Meschini I, Nobili F, Mancini M, Marassi R, Tossici R, Savoini A, Focarete ML, Croce F (2013) High-performance Sn@carbon nanocomposite anode for lithium batteries. J Power Sources 226:241–248
42. Lu W, Luo C, Li Y, Feng Y, Feng W, Zhao Y, Yuan X (2013) CoSn/carbon composite nanofibers for applications as anode in lithium-ion batteries. J Nanopart Res 15:1–11
43. Li X, Zhong Y, Cai M, Balogh MP, Wang D, Zhang Y, Li R, Sun X (2013) Tin-alloy heterostructures encapsulated in amorphous

carbon nanotubes as hybrid anodes in rechargeable lithium ion batteries. Electrochim Acta 89:387–393
44. Song X (2013) A hierarchical hybrid design for high performance tin based Li-ion battery anodes. Nanotechnology 24:205401
45. Zhou X, Zou Y, Yang J (2013) Carbon supported tin-based nanocomposites as anodes for Li-ion batteries. J Solid State Chem 198:231–237
46. Zhuo K, Jeong MG, Chung CH (2013) Highly porous dendritic Ni–Sn anodes for lithium-ion batteries. J Power Sources 244:601–605
47. Wei Z, Mao H, Huang T, Yu A (2013) Facile synthesis of Sn/TiO_2 nanowire array composites as superior lithium-ion battery anodes. J Power Sources 223:50–55
48. Chen X, Guo J, Gerasopoulos K, Langrock A, Brown A, Ghodssi R, Culver JN, Wang C (2012) 3D tin anodes prepared by electrodeposition on a virus scaffold. J Power Sources 211:129–132
49. Wu M, Wang C, Chen J, Wang F, Yi B (2013) Sn/carbon nanotube composite anode with improved cycle performance for lithium-ion battery. Ionics 19:1341–1347
50. Dimov N, Xia Y, Yoshio M (2007) Practical silicon-based composite anodes for lithium-ion batteries: fundamental and technological features. J Power Sources 171:886–893
51. Tamura N, Ohshita R, Fujimoto M, Fujitani S, Kamino M, Yonezu I (2002) Study on the anode behavior of Sn and Sn–Cu alloy thin-film electrodes. J Power Sources 107:48–55